Fluctuations of a membrane nanotube revealed by high-resolution force measurements

F. Valentino, Pierre Sens, J. Lemière, A. Allard, T. Betz, Clément Campillo, C. Sykes

▶ **To cite this version:**

F. Valentino, Pierre Sens, J. Lemière, A. Allard, T. Betz, et al.. Fluctuations of a membrane nanotube revealed by high-resolution force measurements. Soft Matter, 2016, 12 (47), pp.9429 - 9435. 10.1039/c6sm02117d . hal-01411519

HAL Id: hal-01411519

https://hal.sorbonne-universite.fr/hal-01411519

Submitted on 7 Dec 2016

HAL is a multi-disciplinary open access archive for the deposit and dissemination of scientific research documents, whether they are published or not. The documents may come from teaching and research institutions in France or abroad, or from public or private research centers.

L'archive ouverte pluridisciplinaire **HAL**, est destinée au dépôt et à la diffusion de documents scientifiques de niveau recherche, publiés ou non, émanant des établissements d'enseignement et de recherche français ou étrangers, des laboratoires publics ou privés.

Soft Matter

ARTICLE

Fluctuations of a membrane nanotube revealed by high-resolution force measurements

Received 00th January 20xx,
Accepted 00th January 20xx

DOI: 10.1039/x0xx00000x

www.rsc.org/softmatter

F. Valentino[a,b,c], P. Sens[a,b], J. Lemière[a,b,c,1], A. Allard[a,b,e], T. Betz[d], C. Campillo[e,*], and C. Sykes[a,b,*]

Abstract: Pulling membrane nanotubes from liposomes presents a powerful method to gain access to membrane mechanics. Here we extend classical optical tweezers studies to infer membrane nanotube dynamics with high spatial and temporal resolution. We first validate our force measurement setup by accurately measuring the bending modulus of EPC membrane in tube pulling experiments. Then we record the position signal of a trapped bead when it is connected, or not, to a tube. We derive the fluctuation spectrum of these signals and find that the presence of a membrane nanotube induces higher fluctuations, especially at low frequencies (10-1000 Hz). We analyse these spectra by taking into account the peristaltic modes of nanotube fluctuations. This analysis provides a new experimental framework for a quantitative study of the fluctuations of nanotubular membrane structures that are present in living cells, and now classically used for *in vitro* biomimetic approaches.

1 Introduction

Liposomes, also called Giant Unilamellar Vesicles (GUVs), are spherical cell-sized objects made of a single lipid bilayer. They constitute a powerful tool in cell biophysics as bioreactors to mimic living cells[1] which allow for a bottom-up reconstitution of cell architecture and in particular the study of membrane-cytoskeleton mechanics in controlled conditions[2]. The mechanics of such objects can be characterized by pulling membrane nanotubes from liposomes, as in the pioneering experiments of Evans[3]. Understanding the dynamics of such tubes is important from a practical point of view, because there are increasingly being used to probe cell mechanics, but also because they mimic the geometry of filopodia and traffic intermediates.

Membrane nanotubes are formed when a high enough point force is applied perpendicularly to a liposome membrane. It has already been shown that the force necessary to pull a membrane tube depends on membrane mechanics (tension, bending elasticity modulus[4], viscosity[5]). Most tube pulling experiments rely on micropipette aspiration of the liposome to fix membrane tension, while the tube is pulled by a microbead trapped in an optical tweezer system[5–7]. The force F on the tube can be related to the stiffness of the optical trap $ktrap$ and the bead displacement from the trap centre d: $F = k_{trap}d$. Here, we use a back focal plane aligned Quadrant PhotoDiode (QPD)[8,9] to detect relative bead displacements and Acousto-Optical Deflectors (AODs) to rapidly move the laser focus. The QPD allows for the recording of the bead motion relative to the laser focus with a high temporal resolution[10–13] of up to 4 microseconds, well under the resolution of video-tracking (typically a few tens of milliseconds[14]). Hence, the force is measured with a sub pico-newton resolution.

First, we measure the force needed to hold nanotubes pulled out from liposome membranes and validate our force detection by the accurate measurement of membrane bending modulus. We show that our method allows for direct comparison of trapped bead fluctuations either attached to a membrane nanotube, or standing in solution. We can therefore, for the first time, infer the sole effect

[a] Institut Curie, PSL Research University, CNRS, UMR 168, 75005 Paris, France.
[b] Sorbonne Universités, UPMC Univ Paris 06, 4 place Jussieu, 75005 Paris, France.
[c] Univ Paris Diderot, Sorbonne Paris Cité, 5 rue Thomas-Mann, 75205 Paris, France.
[d] Institute of Cell Biology, Center for Molecular Biology of Inflammation, Cells-in-Motion Cluster of Excellence, Münster University, Von-Esmarch-Strasse 56, D-48149 Münster, Germany.
[e] Université Evry Val d'Essonne, LAMBE, Boulevard F Mitterrand, Evry 91025, France.
[1] Present address: Department of Molecular Biophysics and Biochemistry, Nanobiology Institute, Yale University, New Haven, CT, USA.
[*] Corresponding authors: clement.campillo@univ-evry.fr; cecile.sykes@curie.fr

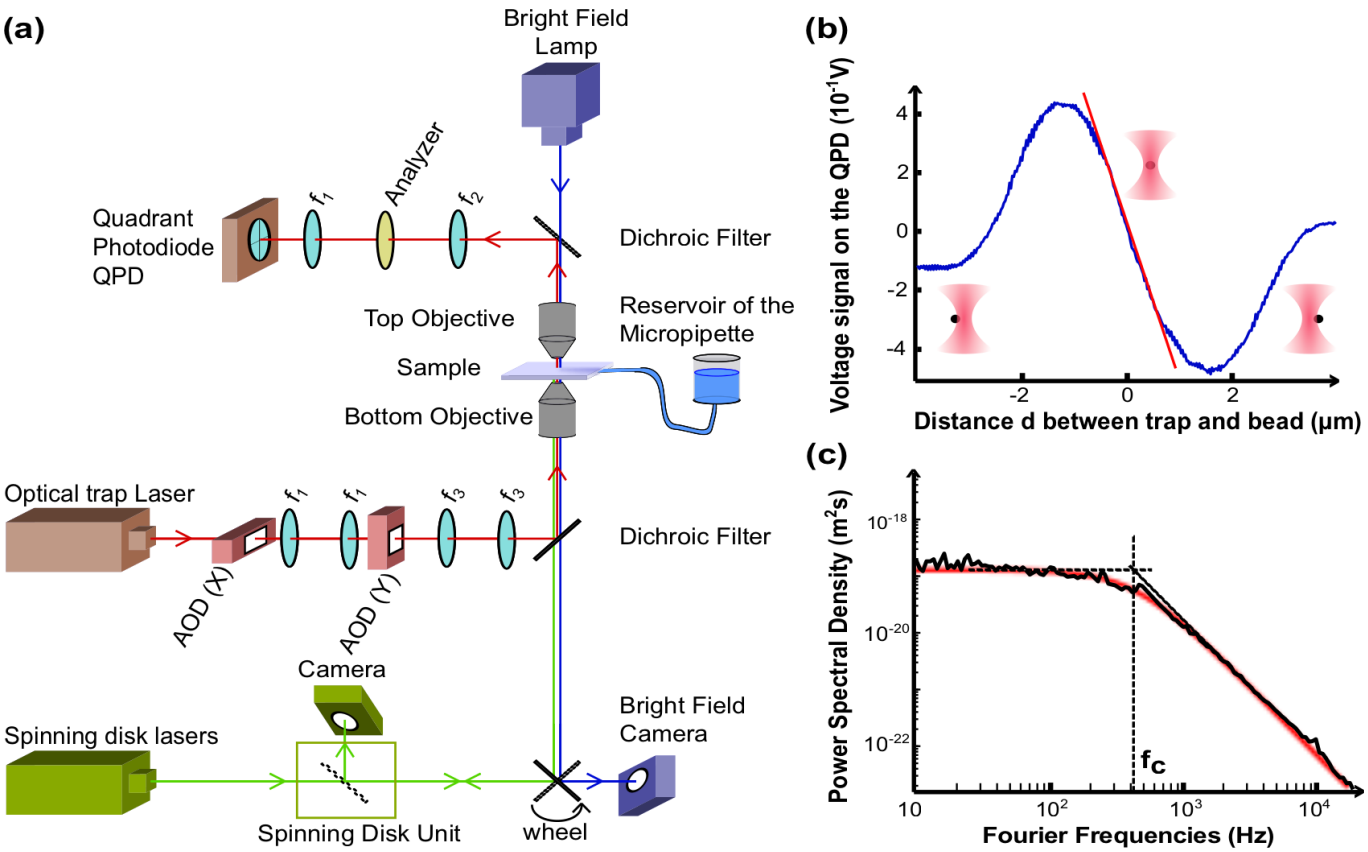

Fig. 1 (a) **Scheme of the tube pulling set-up.** The optical trap laser (red line) controlled by Acousto-Optical-Deflectors (AOD), interacts with the sample and is analyzed with a Quadrant PhotoDiode (QPD). Fluorescent signals are recorded using a spinning disk microscopy unit. The spinning disk lasers and the bright Field optical pathways are respectively represented in green and blue. (b) **QPD calibration**. The voltage signal on the QPD is recorded as the trap is moved rapidly to scan a bead (see Materials and method 2.7). The linear regime fitted by the red line provides the QPD calibration. Here the slope value is $(-0.42 \pm 0.01)\ \mathrm{V.\mu m^{-1}}$. (c) **Trap stiffness calibration**. A Lorentzian curve (red) is fitted to the Power Spectral Density (black) of the position of a bead that evolves freely in the optical trap. In this case, k_{trap} is $41\ \mathrm{pN.\mu m^{-1}}$.

of fluctuations of membrane nanotubes. We find that at low frequencies (10-1000 Hz), the fluctuation of the bead position is increased when a tube is attached, an effect that can be explained by radius fluctuations of the tube. Our work paves the way to a new characterisation of membrane nanotubes that may reveal new features previously hidden, due to experimental time resolution limitations.

2 Materials and methods

2.1 Lipids, reagents and buffers

EPC (L-α-phosphatidylcholine from egg yolk) and biotinylated lipids (1,2-distearoyl-sn-glycero-3-phosphoethanolamine-N-[biotinyl(polyethylene glycol) 2000]), are purchased from Avanti Polar Lipids (Alabaster, USA). Beads are polystyrene, streptavidin-coated beads 0.5% w/v 3.05 µm diameter from Spherotech,(Illinois, USA). The commercial solution is diluted 500 times.

Different inside and outside buffers are used. The internal buffer consists in 20 mM HEPES (pH 7), 100 mM sucrose and 10 µg.L^{-1} Sulforhodamine B. The external buffer contains 10 mM HEPES (pH 7), 50 µM $CaCl_2$, 1 µM dithiothreitol (DTT), 0.5 mM diazabicyclo[2,2,2]octane (DABCO), 2 mM $MgCl_2$, 5 mM ATP, 50 mM KCl, and 70 mM glucose.

Both buffers are set at 7 pH. Osmolarity (Vapro 5600, WESCOR, USA) of the internal buffer is 170 mOsm.L^{-1} and external buffer is 200 mOsm.L^{-1} to have an external buffer slightly more concentrated and allow for liposome deflation ($\Delta Osm = +30\ \mathrm{mOsm.L^{-1}}$).

2.2 Liposome formation

Liposomes are formed using the standard electroformation method[15]. The lipid mix (molar ratio 99% EPC / 1% biotinylated lipids) is dissolved at 2.5 g.L^{-1} in chloroform/methanol at a volume ratio of 5/3. A volume of 4 µL of this solution is spread on an ITO-coated (Indium Tin Oxide) glass slide (63691610PAK, Sigma Aldrich, Germany). The slides are stored in a vacuum chamber for 2 hours to evaporate the solvent. Then two slides are assembled into a chamber, their conductive sides facing each other, filled with the internal buffer and sealed with Vitrex© (Vitrex Medical A/S, Denmark). An alternative electric field (10 Hz, 2.3 V peak to peak) is applied across the chamber over night. Liposomes can be stored at 4°C for up to a week.

2.3 Micropipette preparation

Micropipettes are obtained from borosilicate capillaries (0.7/1.0 mm inner/outer diameter, Kimble, USA), using a puller (P2000, Sutter Instrument, USA) with parameters: Heat 360, Pull 100,

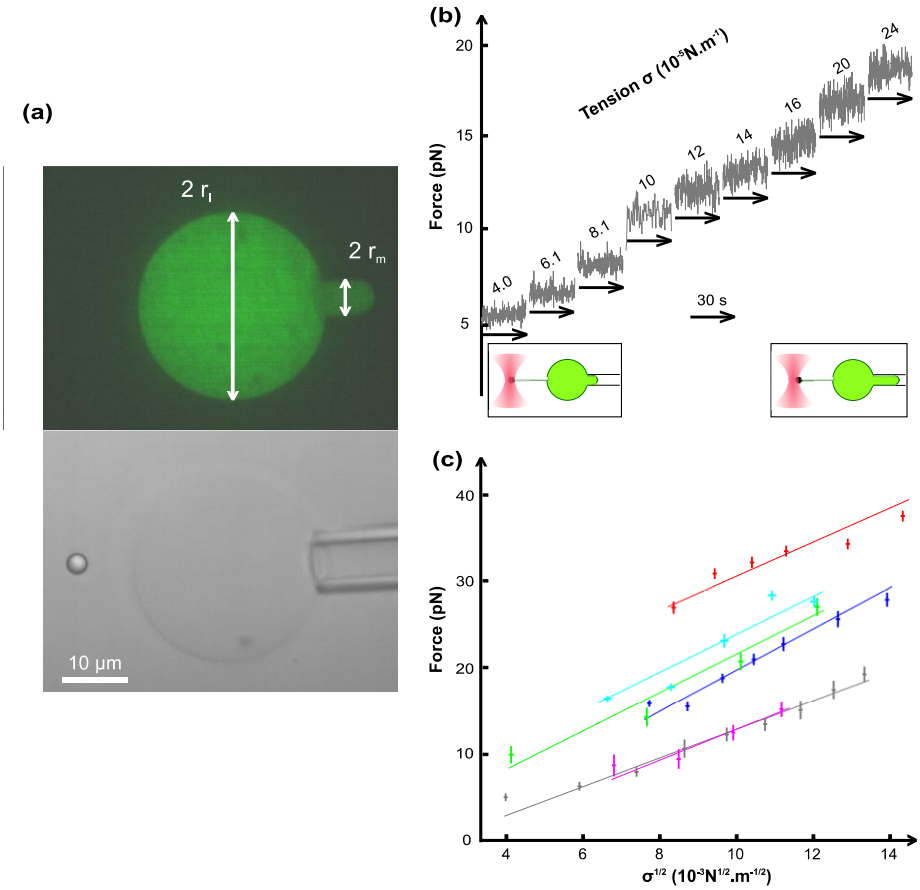

Fig. 2 (a) **View of the experiment**. A liposome observed by confocal (top) and bright field illumination (bottom) filled with sulforhodamine B (green) and held in a micropipette. (b) **Force measurements**. Evolution of the force on a bead in a tube pulling experiment at different fixed tension, with a fixed tube length of 8 µm. The force for each tension is recorded during 30 s. Experiments are done with $k_{trap} = (37 \pm 6)\ \mathrm{pN.\mu m^{-1}}$. (c) **Bending modulus measurements**. Forces as a function of $\sigma^{1/2}$ for 6 different liposomes. The fitted lines give access to the bending modulus (κ) of the liposome through the slope $2\pi\sqrt{2\kappa}$ (see Eq.4).

Velocity 30, Fil 4, Del 180. Micropipette tips are then micro-forged (MF 830, Narishig, Japan) up to 5-6 µm internal diameter. Just before experiments, they are filled with a passivation buffer containing 0.5 g.L^{-1} β-casein (C6905, Sigma Aldrich, Germany) diluted in water and adjusted at pH 7 using caustic soda.

2.4 Chamber preparation

The experimental chamber is made of two glass coverslips (0.13-0.16 mm, Menzel Gläze, Australia) separated by a 1 mm layer of steel. The total volume of such a chamber is 200 µL. Walls of the chamber and the outside of the aspiration micropipette are passivated with 5 g.L^{-1} β-casein diluted in water by incubation for 15 minutes. This solution is then aspirated by a tissue paper (Kimtech©, Kimberly-Clark, USA) and replaced by the external buffer. Beads (1 µL) and liposomes (10 µL from the electroformation solution) are added. The micropipette is positioned in the focus plane of the objective inside the chamber. The pressure inside the micropipette is then fixed to zero by adjusting the height h of the reservoir (Fig. 1(a)) to stop any liquid flow in the micropipette. After aspirating a liposome, its tension σ can be modified according to the Laplace law by changing the aspiration of the micropipette (Eq. 1), which can be done by modifying the height h of the reservoir (counted as positive if the reservoir is lowered):

$$\sigma = \frac{1}{2}\,\rho\, g\, |h|\, r_m \left(1 - \frac{r_m}{r_l}\right)^{-1} \qquad (1)$$

ρ is the density of the aspirating fluid (here water), r_m the radius of the micropipette, and r_l the radius of the liposome. Finally, the chamber is sealed by mineral oil (8042-47-5, Sigma Aldrich, Germany) to prevent evaporation.

2.5 Optical tweezers

~~A major advantage of our method is that we rapidly calibrate the trap stiffness and measure forces *in situ* during each experiment. The calibration is done directly on the bead used for tube pulling and we hence avoid systematic errors due to bead polydispersity.~~

The setup, as shown in Fig. 1(a), consists in an Infra Red (IR) laser ($\lambda = 1064\ \mathrm{nm}$, $P = 5\ \mathrm{W}$, YLM-5-LP-SC, IPG Laser, Germany) which is intensity - and direction - controlled by an XY AOD pair (MT80- A1, 51064 nm, AA Opto Electronic, France). Two lenses ($f_1 = 50\ \mathrm{mm}$) are put between the AODs for a correct conjugation. The beam is then injected into the microscope (Eclipse Ti, Nikon, Japan) by a dielectric mirror (Beamsplitter, AHF, Germany). The light is focused by the bottom water immersion objective (PLAN APO VC 60xA/1.2WI OFN 25 DIC N2, Nikon, Japan) on the sample, mounted on a 2D piezo stage for precise sample positioning (MS 2000, ASI, USA). After interaction with the sample, the light is collected by the top water immersion objective (NIR APO

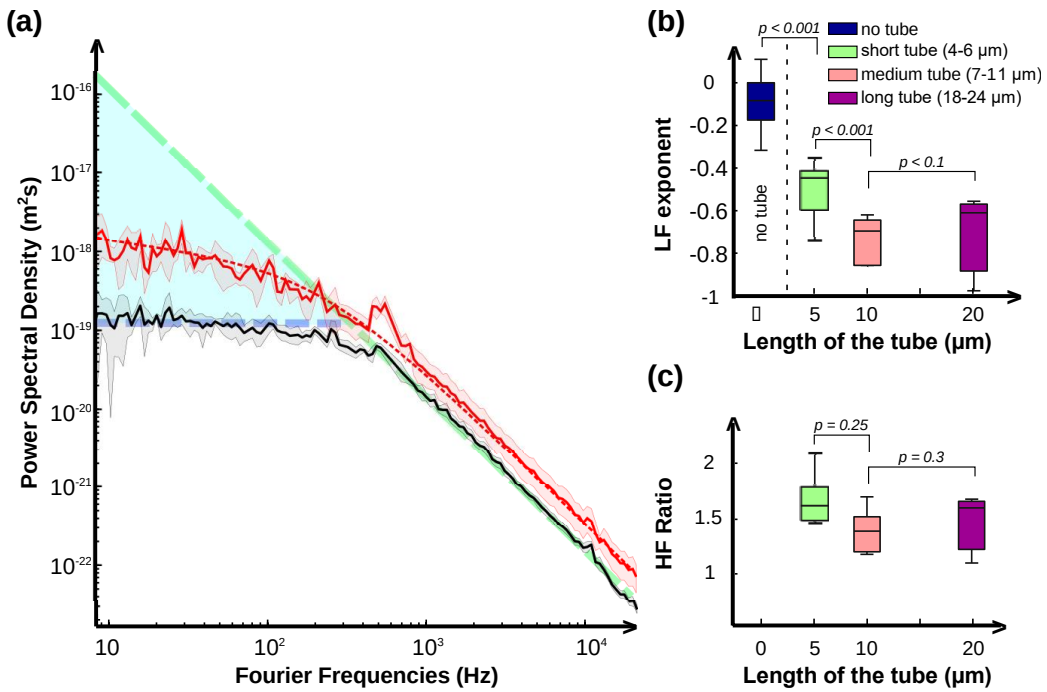

Fig. 3 (a) **Comparison of PSDs**. Example of a PSD of a free bead (black) as the liposome / micropipette system is far from the bead (> 15 µm) and the same bead attached to a tube (red). Dashed red line is obtained by fitting the curve according to Eq. 10. The tube is 9.0 µm long, $k_{trap} = 38\,\mathrm{pN.\mu m^{-1}}$, and slopes measured at $(-0.27 \pm 0.01)\,\mathrm{V.\mu m^{-1}}$ with a tube, and $(-0.26 \pm 0.01)\,\mathrm{V.\mu m^{-1}}$ without. (b) **LF exponent at different lengths**. Exponent of the PSD measured between 10 and 200 Hz as a function of the length of the pulled tube. P-values are obtained by t-test ($N = 9$ independent experiments). (c) **HF Ratio at different lengths**. Ratio $PSD_{tube}/PSD_{freebead}$ measured between 1 kHz and 10 kHz ($n = 9$). This ratio is 1 (not shown) for a free bead.

60x/0.80W DIC N2, Nikon, Japan) that acts as a condenser. A mirror reflects the beam, and two lenses ($f_2 = 150$ mm, $f_3 = 100$ mm) image the back focal plane of the top objective on a QPD (PDQ-30-C, Thorlabs, Germany). To adjust the intensity of the laser on the QPD without changing the stability of the laser, an analyzer is added.

The optical tweezer is controlled by a custom written control program (Labview 2011, National Instruments, USA). A frequency generator and a high frequency amplifier respectively control the AODs by the analogic channels of two data acquisition cards (NI-DAQ 6363, National Instruments, USA), to adjust the position and the trap stiffness. The analog input of the same cards reads the voltage signals from the QPD. The synchronization of both signal generation and acquisition is performed at 250 kHz: 2 µs is the shortest time resolution for our set-up.

2.6 Image acquisition

Images obtained by bright field illumination are recorded by a CMOS Camera (DCC 1545 M-GL, Thorlabs, Germany). Images obtained by confocal laser illumination (CSUX1 Yokogawa, Andor Technology, Ireland) are recorded by a high resolution sCMOS Camera (Andor Neo, Ireland). A motorized prism ensures the switch from one to the other.

2.7 QPD calibration

Classically, the position *d* of the bead is measured by video tracking and is thus limited in spatial and temporal resolution[16]. A major advantage of our method is that we rapidly calibrate the QPD signal ~~trap stiffness and~~ that can be used to measure forces *in situ* during each experiment. The calibration is done directly on the bead used for tube pulling and we hence avoid systematic errors due to bead polydispersity. Here, the back focal plane technique, based on interference of the light scattered and unscattered by the bead[9], allows us to obtain a voltage signal on the QPD, V_{QPD} on Fig. 1(b), proportional to the relative position *d* of the bead to the centre of the trap. We calibrate the voltage to µm ration of V_{QPD} by controlled and fast (4 µs) variation of the laser focus position *d* using the AODs while recording V_{QPD}. During this short time, the bead is submitted to a maximal force of 80 pN that corresponds to a maximal displacement of 8 nm, so the bead is well immobile as $V_{QPD}(d)$ is recorded. To ensure that the bead position can equilibrate at the trap centre, we maintain the trap immobile for 100 µs at the central position before visiting a new position. This procedure[17] is repeated for -3 µm < d < 3 µm with a stepsize of 20 nm to get a complete scan as shown in Fig. 1(b). The linear regime is fitted to obtain the conversion $V_{QPD}(d)$. Whole QPD calibration takes 1.2 second and is performed before each measurement, *in situ*.

2.8 Trap stiffness k_{trap} calibration

The trap stiffness k_{trap} is often assessed by applying a series of known frictional forces on the bead and measuring its displacement. In our approach, when the bead is optically trapped, it is submitted to the trap force, the viscous Stokes force, and the fluctuation (Brownian) force that varies in time $\Gamma(t)$. Thus, the distance between the centre of the bead and the centre of the trap follows a Langevin equation Eq. (2), where η is the dynamic viscosity of water, r_{bead} the radius of the bead, and $\dot{d}$ the time derivative of d.

$$k_{trap}d(t) + 6\pi\eta r_{bead}\dot{d}(t) = \Gamma(t) \quad (2)$$

Using the Fourier transform, we can get[17] the Power Spectral Density (PSD) of the position of the bead (relative to the centre of the optical trap) as shown in Eq. (3), where T_{exp} is the duration of the experiment. Trap linearity is checked by applying a Stokes force to the bead displaced at an imposed velocity (Fig. S1). Note that measuring k_{trap} through bead fluctuations and imposed Stokes forces gives identical results.

$$PSD(f) = \frac{\left|\tilde{d}^2(f)\right|}{T_{exp}} = \frac{1}{T_{exp}} \frac{\left|\tilde{\Gamma}^2\right|/k_{trap}^2}{1 + f^2/f_c^2}\ ,\ f_c = \frac{k_{trap}}{12\,\pi^2\eta r_{bead}} \quad (3)$$

With $\left|\tilde{\Gamma}^2\right| = 12\pi\eta r_{bead} k_B T\, T_{exp}$. To obtain the corner frequency f_c the PSD of the trapped bead position is fitted by a Lorentzian as seen in Fig. 1(c) to extract k_{trap}. We measure the trap stiffness before each experiment, on average it is (37 ± 6) pN.µm^{-1} for a laser power of 80 mW on the sample. All fits are obtained by Matlab R2012b (8.0.0.783).

3 Results

3.1 Tube pulling experiments

First, we want to validate our experimental force detection by pulling membrane nanotubes from liposomes. We thus measure the bending modulus of their membrane, and then compare the obtained values to published ones. The experiment procedure is as follows: we aspirate a liposome with a micropipette, at a fixed tension set by h Eq. (1). A membrane tongue is created in the micropipette Fig. 2(a). Then, we catch a free bead with the optical tweezer and calibrate the signal of the QPD ($V_{QPD}(d)$ and k_{trap}, see Materials and methods and Fig. 1(b and c)). The liposome is slowly approached to touch the bead, and then pulled away to form a nanotube of more than 1 µm, over the threshold of nucleation of a cylindrical tube at a fixed membrane tension, as already described both experimentally[18] and theoretically[19]. Then, $V_{QPD}(d)$ is calibrated again in the presence of the tube for an accurate measurement of the bead distance to the trap centre, *d*.

The evolution of the force exerted on the bead is recorded as a function of time. Fluctuations of the force are observed on a 30 second time frame (Fig. 2(b)). Membrane tension is increased stepwise by lowering the altitude h of the reservoir, which increases the aspiration pressure. A pause of 30 s is made between each step to let the system relax to its equilibrium. Theoretically, the equilibrium force to maintain a nanotube is given by Eq. (4)[20].

$$F = 2\pi\sqrt{2\kappa_b\sigma} \quad (4)$$

Where σ is the membrane tension of the liposome, and κ_b the bending modulus of the membrane. We observe that the average force increases with tension, in qualitative agreement with Eq. (4). Moreover, we find that the force is proportional to $\sigma^{1/2}$ Fig. 2(c), and using Eq. (4) gives an estimate of the bending modulus of (8.6 ± 2.4) k_bT. This value is in accordance with published values for EPC membranes[21,22], demonstrating the validity of our experimental system for equilibrium force measurements.

3.2 Nanotube fluctuations

To take advantage of the high temporal and spatial resolution of our tube pulling setup, we now address how bead fluctuations are modified by the presence of a membrane nanotube attached to its surface. Fig. 2(b) already shows that increasing tension leads to an increase in force fluctuation amplitude. This observation prompted us to characterize these fluctuations in more detail.

The fluctuations of the same bead, in the absence (free bead) or in the presence of a membrane tube, are recorded after a new $V_{QPD}(d)$ calibration (see Material and methods). The linear dependence of the QPD voltage $V_{QPD}(d)$ as a function of bead position in the trap is systematically checked (see Material and methods) in the presence and in the absence of the membrane nanotube (Fig. S2). As can be observed in Fig. S2, the slopes of this linear regime slightly differ, and we take into account each relevant value for an accurate determination of bead position. Bead fluctuations can then be recorded in the absence or in the presence of a membrane nanotube and we show that the amplitude of bead fluctuations increases when a nanotube is present (Fig. S3-4). This is confirmed by standard deviation estimates in the presence of a tube (Fig. S5). Moreover, these amplitudes slightly increase when the tube is longer (Fig. S3) or when membrane tension is higher (Fig. S4).

Bead fluctuations are then processed into a PSD curve as a function of frequency (Fig. 3(a), free bead, black; same bead attached to a nanotube, red). As expected, the free bead curve can be fitted by a Lorentzian (Fig. 1(c), Eq. 3) and shows a plateau at low frequency (blue dashed line Fig. 3(a)) and a (-2) exponent at high frequency (green dashed line Fig. 3(a)), in agreement with Eq. (3). Strikingly, the PSD obtained in the presence of a membrane tube is very different from the one of a free bead, and also from the one of a bead bound to the membrane in the absence of tube (Fig. S6). At low frequencies, the PSD of a membrane tube radically differs from the plateau behaviour of a free bead; to characterize this behaviour at low frequencies we fit the PSD curve between 10 and 200 Hz by a simple power law and obtain a low frequency exponent called "LF exponent". At high frequencies, we obtain parallel curves, indicating that the (-2) exponent is unchanged whereas there is a shift of the PSD curve in the presence of a membrane tube). In order to quantify this shift, we measure the ratio of the PSD in the presence versus in the absence of the membrane tube $PSD_{tube}/PSD_{freebead}$ at high frequencies (between 1 and 10 kHz) and we call this high frequency ratio "HF ratio".

Both LF exponent and HF ratio characterize the fluctuations of the bead either in the absence or in the presence of a membrane tube. Whereas the LF exponent is found to be close to zero for a free bead (Fig. 1(c), S7), we find that it decreases to (-0.5) for a tube with an average length of 4 µm (Fig. 3(b), S7). Varying the length of the tube while keeping membrane tension constant does not alter the average value of the force (Eq. (4)). It only slightly alters the HF ratio (Fig. 3(c)) and the LF exponent (-0.7).

Keeping tube length constant and varying membrane tension also leads to a modification of the PSD curve (Fig. S8). We find indeed that the HF ratio drastically increases with tension (Fig. S9) whereas the LF exponent does not significantly change (Fig. S10).

Discussion

Our setup allows for a correct determination of bending elasticity modulus, thus validating the tube pulling procedure. Furthermore, we take advantage of the possibility to calibrate the bead position *in situ* before each experiment, to record an accurate value of bead position as a function of time. Our setup therefore leads to unprecedented precision on tube fluctuations. The precision of our setup relies on two facts: 1) that we use a QPD and back focal plane technique developed for optical tweezers systems[9] and 2) that we are able to calibrate the exact bead that is used for a tube pulling experiment and compare the same bead in a free state and once attached to a membrane tube.

The PSD of a free bead has two regimes depending on the frequency. At high frequency (1-10 kHz), Eq. (3) leads to Eq. (5), where the exponent (-2) represents the purely viscous regime.

$$PSD_{HF}(f) = \frac{1}{T_{exp}} \frac{\left|\tilde{\Gamma}^2\right|/k_{trap}^2}{f^2/f_c^2} \quad (5)$$

At low frequency, Eq. (3) leads to Eq. (6); the plateau (LF exponent is equal to zero) corresponds to the elastic regime of the bead in a trap.

$$PSD_{LF}(f) = \frac{1}{T_{exp}} \left|\tilde{\Gamma}^2\right|/k_{trap}^2 \quad (6)$$

The presence of a membrane tube has two major effects, one at low, one at high frequency. Note that the PSD of a bead bound to the membrane (without a tube) only slightly differs from the PSD of a free bead PSD (Fig. S6 and [23]) compared to the situation with a tube. We find that at low frequency, the LF exponent drastically differs from zero in the presence of a tube (Fig. 3(a)). This effect shows that the pure elastic regime is no longer valid. We define a viscous-elastic triangle delimitated by the viscous regime (green dashed line Fig. 3(a) with exponent (-2)) and the elastic regime (blue dashed line with exponent (0)). The PSD in the presence of a tube appears in this triangle, thus indicating a viscous component. At high frequency, the PSD in the presence of a tube is systematically positioned above the free bead PSD. This shift still needs to be understood.

In order to derive the PSD of a bead attached to a fluctuating tube, we make use of the Fluctuation-Dissipation Theorem (FDT), which relates the PSD $S_l(f)$, to the mechanical response function $\chi(f)$, itself linking the variation of the tube extension $\delta x(f)$ to a small force $\delta F(f)$ applied to the end of the tube ($\delta l_f = \chi_{tube}(f)\delta F_f$). The FDT reads[24]:

$$S_x(f) = \frac{k_B T}{\pi f} Im[\chi(f)] \quad (7)$$

The dynamics of membrane tube fluctuations are quite complicated, and involve a combination of peristaltic (squeezing) modes, where the tube remains axisymmetrical but its radius changes, and bending modes, where the tube radius remains constant, but its axis undulates[25]. Another complication is that the variation of the tube shapes involves both membrane and solvent transfer between the tube and the liposome from which it is pulled. Here, we use an approximate expression of the tube mechanical response function that focuses on the peristaltic modes and assumes membrane area is not transferred between the tube and the liposome, as should be appropriate for the high frequency response. In this limit, the response function is related to the oscillation frequency according to[26]:

$$\chi_{tube}(f) = \frac{tanh\, q_f\, L}{q_f\, F}, q_f = \sqrt{\frac{2\pi f}{i\, D_r}}, D_r = \frac{F}{32\pi\eta_I} \quad (8)$$

Here, F is the average tether force (Eq. (4)), L the average tube length, and η_I the viscosity of the solvent inside the tube. The dynamics of tube relaxation is thus controlled by a "diffusion coefficient" D_r, which taking $F_0 = 20$ pN and $\eta_I = 10^{-3}$ Pa.s, is of order $D_r = 200\ \mu m^2 s^{-1}$. This response function depends on the tube length L. However, this dependency disappears in the limit $|q_f L| \gg 1$, that is in the limit of high frequency, where a perturbation at the open end of the tube decays exponentially over a length $\sim 1/|q_f|$ much smaller than the tube length. The crossover frequency is given by $f_L = D_r/2\pi L^2$, which is of order 0.3 Hz for $L = 10\ \mu m$, so the tube length should not affect the mechanical response function for the frequency range reported here.

The full response function χ is obtained considering the tether acts on the bead in parallel with the visco-elastic environment (solvent plus optical trap), so that:

$$\chi = \frac{1}{1/\chi_{trap} + 1/\chi_{tube}} = \frac{1}{12\pi^2\eta r_{bead}} \frac{1}{f_c + if + (1+i)\sqrt{f_t f}} \quad (9)$$

$$\text{with } f_t = \frac{F^2}{4\pi D_r (6\pi\eta r_{bead})^2} = \frac{2}{9}\frac{F\eta_I}{(\pi\eta r_{bead})^2}$$

Finally, the PSD is:

$$S_l(f) = \frac{k_B T}{12\pi^3\eta r_{bead}} \frac{1+\sqrt{f_t/f}}{\left(f_c + \sqrt{f_t f}\right)^2 + \left(f + \sqrt{f_t f}\right)^2} \quad (10)$$

This PSD is thus characterised by two parameters: the trap cutoff frequency f_c, and the "tube" frequency f_t. Using values of the trap stiffness $k_{trap} = 40$ pN.μm^{-1}, $F = 20$ pN and $r_{bead} = 1.5\ \mu m$, values corresponding to Fig. 3(a), we calculate $f_c = 225$ Hz and $f_t = 200$ Hz. This shows that the typical tube frequency is expected to be of the same order than the cut-off frequency. One thus expects the tube dynamics to strongly influence the fluctuation spectrum of the bead in the frequency range of interest. At low frequency, Eq. (10) leads to $S_l(f) \sim \sqrt{f_t}/(f_c{}^2\sqrt{f})$ thus a low-frequency exponent of -0.5, close to the value we obtained for short tubes and in qualitative agreement with our observation for all tether lengths (Fig. 3(b)).

The model that includes only peristaltic modes of tether deformation allows for qualitative explanation of our observations, namely an increase of the amplitude of low-frequency oscillations and a high-frequency response dominated by the viscous drag on the bead. Further refinement would be needed to fully explain our experimental data, as the fitted values correspond to $f_t = f_c/5$ (30 and 150 Hz for Fig. 3(a), the same trend is observed in $N = 9$ experiments) while our estimate suggests $f_t \sim f_c$.

Conclusions

We have built a system that allows formation of membrane nanotubes using an *in situ* calibration of force measurements. We have validated this approach by accurate measurements of liposome membrane bending moduli. Moreover, this set-up allows us to record the force fluctuations of membrane nanotubes at an unprecedented high frequency. We show that the fluctuations spectrum of a bead attached to a membrane nanotube exhibits a modification at low frequency that we explain by tube radius fluctuations. The understanding of tube dynamics is important from a practical point of view, because membrane tubes are increasingly being used to probe cell mechanics, but also because they mimic the geometry of filopodia and traffic intermediates. This work paves the way for further studies in particular of nanotubes submitted to active fluctuations that are present in cells.

Acknowledgements

This work was supported by the French Agence Nationale pour la Recherche (ANR), grant ANR 09BLAN0283 and ANR 12BSV5001401, and by the Fondation pour la Recherche Médicale (FRM), grant DEQ20120323737.

References

1 K. Carvalho, F.-C. Tsai, E. Lees, R. Voituriez, G. H. Koenderink and C. Sykes, *Proc. Natl. Acad. Sci.*, 2013, **110**, 16456–16461.
2 K. Guevorkian, J. Manzi, L.-L. Pontani, F. Brochard-Wyart and C. Sykes, *Biophys. J.*, 2015, **109**, 2471–2479.
3 E. Evans and A. Yeung, *Chem. Phys. Lipids*, 1994, **73**, 39–56.
4 A. Roux, *Soft Matter*, 2013, **9**, 6726.
5 O. Rossier, D. Cuvelier, N. Borghi, P. H. Puech, I. Derényi, A. Buguin, P. Nassoy and F. Brochard-Wyart, *Langmuir*, 2003, **19**, 575–584.
6 B. Sorre, A. Callan-Jones, J. Manzi, B. Goud, J. Prost, P. Bassereau and A. Roux, *Proc. Natl. Acad. Sci.*, 2012, **109**, 173–178.
7 C. Campillo, P. Sens, D. Köster, L.-L. Pontani, D. Lévy, P. Bassereau, P. Nassoy and C. Sykes, *Biophys. J.*, 2013, **104**, 1248–1256.
8 P. Ramesh, Y. F. Baroji, S. N. S. Reihani, D. Stamou, L. B. Oddershede and P. M. Bendix, *Sci. Rep.*, 2013, **3**.
9 F. Gittes and C. F. Schmidt, *Opt. Lett.*, 1998, **23**, 7.
10 K. C. Vermeulen, J. van Mameren, G. J. M. Stienen, E. J. G. Peterman, G. J. L. Wuite and C. F. Schmidt, *Rev. Sci. Instrum.*, 2006, **77**, 13704.
11 F. Gittes, B. Schnurr, P. D. Olmsted, F. C. MacKintosh and C. F. Schmidt, *Phys. Rev. Lett.*, 1997, **79**, 3286–3289.
12 T. Bornschlogl, S. Romero, C. L. Vestergaard, J.-F. Joanny, G. T. Van Nhieu and P. Bassereau, *Proc. Natl. Acad. Sci.*, 2013, **110**, 18928–18933.
13 S. F. Tolić-Nørrelykke, E. Schäffer, J. Howard, F. S. Pavone, F. Jülicher and H. Flyvbjerg, *Rev. Sci. Instrum.*, 2006, **77**, 103101.
14 C. Prévost, H. Zhao, J. Manzi, E. Lemichez, P. Lappalainen, A. Callan-Jones and P. Bassereau, *Nat. Commun.*, 2015, **6**, 8529.
15 M. I. Angelova and D. S. Dimitrov, *Faraday Discuss. Chem. Soc.*, 1986, **81**, 303.
16 M. Bretou, O. Jouannot, I. Fanget, P. Pierobon, N. Larochette, P. Gestraud, M. Guillon, V. Emiliani, S. Gasman, C. Desnos, A.-M. Lennon-Dumenil and F. Darchen, *Mol. Biol. Cell*, 2014, **25**, 3195–3209.
17 H. Turlier, D. A. Fedosov, B. Audoly, T. Auth, N. S. Gov, C. Sykes, J.-F. Joanny, G. Gompper and T. Betz, *Nat. Phys.*, 2016, **12**, 513–519.
18 A. Roux, D. Cuvelier, P. Nassoy, J. Prost, P. Bassereau and B. Goud, *EMBO J.*, 2005, **24**, 1537–1545.
19 G. Koster, A. Cacciuto, I. Derényi, D. Frenkel and M. Dogterom, *Phys. Rev. Lett.*, 2005, **94**.
20 R. E. Waugh and R. M. Hochmuth, *Biophys. J.*, 1987, **52**, 391–400.
21 S. A. Simon, S. Advani and T. J. McIntosh, *Biophys. J.*, 1995, **69**, 1473–1483.
22 P. Girard, J. Prost and P. Bassereau, *Phys. Rev. Lett.*, 2005, **94**.
23 E. Helfer, S. Harlepp, L. Bourdieu, J. Robert, F. C. MacKintosh and D. Chatenay, *Phys. Rev. E*, 2001, **63**, 21904.
24 R. Kubo, *Rep. Prog. Phys.*, 1966, **29**, 255.
25 K. L. Gurin, V. V. Lebedev and A. R. Muratov, *JETP*, 1996, **83**, 321–326.
26 P. Nassoy, D. Cuvelier, R. Bruinsma and F. Brochard-Wyart, *EPL Europhys. Lett.*, 2008, **84**, 18004.